Analyst

ROYAL SOCIETY OF CHEMISTRY

PAPER

View Article Online
View Journal | View Issue

Cite this: *Analyst*, 2025, **150**, 414

Dual-channel nano-carbon-liquid/liquid junction electrodes for multi-modal analysis: redox-active (dopamine) and non-redox-active (acetylcholine)†

Edappalil Satheesan Anupriya, [a,b] Ran Chen, ‡[a] Daniel Kalski,[a] Jordynn Palmer[a] and Mei Shen *[a,b]

We present here a dual-channel nanoelectrode to detect both redox-active and non-redox-active analytes. The dual-channel nanoelectrode was developed from theta nanopipette. We developed one channel of the theta nanopipette to be a carbon nanoelectrode and the other channel to be a nano interface between two immiscible electrolyte solutions (nanoITIES) electrode, producing a nano-carbon-ITIES platform. The carbon nanoelectrode channel was developed by carbon deposition *via* pyrolysis followed by focused ion beam milling to measure redox-active analytes. The nanoITIES electrode channel was developed to detect non-redox-active analytes. The nano-carbon-ITIES electrodes were characterized using electrochemistry, scanning electron microscopy and transmission electron microscopy. Dopamine (a redox-active analyte) and acetylcholine (a non-redox-active analyte) were measured on the dual-channel nano-carbon-ITIES platform using the carbon nanoelectrode and the nanoITIES electrode, respectively. Using cyclic voltammetry, the diffusion-limited current of dopamine and acetylcholine detection on the nano-carbon-ITIES electrode increased linearly with increasing their concentrations. Using chronoamperometry (current *versus* time), we showed that the nano-carbon-ITIES electrode detected acetylcholine and dopamine at the same time. The introduced first-ever dual-functional nano-carbon-ITIES electrodes expand the current literature in multi-channel electrodes for multi-purpose analysis, which is an emerging area of research. Developing the analytical capability for the simultaneous detection of acetylcholine and dopamine is a critical step towards understanding diseases and disorders where both dopamine and acetylcholine are involved.

Received 29th August 2024,
Accepted 2nd December 2024

DOI: 10.1039/d4an01153h

rsc.li/analyst

Introduction

Developing multi-functional electrodes is one critical step towards multi-purpose electroanalysis. Electrochemically speaking, there are two kinds of analytes, redox-active and non-redox-active. The detection of redox-active analytes is commonly studied on solid electrodes, such as carbon, platinum and gold, through redox reactions. The interface between two immiscible electrolyte solutions (ITIES)[1–24] emerges as a complementary approach in electroanalysis due to its sensitivity to both redox-active and non-redox-active analytes, where the transfer of the charged analyte or the neutral analyte[25] across ITIES generates a faradaic current.[3,9,12,20,26,27] Neurotransmitters,[14,25,28–35] metal ions,[24,36–40] drug molecules,[41–43] and other complex molecules such as proteins[44–47] have been detected using ITIES. To expand the capability of electrochemistry for multi-purpose analysis, we introduce a dual-functional nanoelectrode to detect both redox-active and non-redox-active analytes, simultaneously. Such a dual-functional nanoelectrode (**nano-carbon-ITIES elec-**

[a]*Department of Chemistry, The Beckman Institute for Advanced Science and Technology, University of Illinois Urbana Champaign, Urbana, IL 61801, USA. E-mail: mshen233@illinois.edu*

[b]*Chan Zuckerberg Biohub Chicago, Chicago, Illinois*

†Electronic supplementary information (ESI) available: Electrode modification using FIB milling; radius determination of the carbon channel using cyclic voltammogram (CV) of RuHex; additional cyclic voltammograms exhibiting sigmoidal shape for dopamine detection on the carbon channel of the FIB-milled dual-channel nanoelectrode; radius determination of the nano-ITIES channel using cyclic voltammogram (CV) of TBA; halfwave potential of dopamine detection measured using cyclic voltammogram; cyclic voltammograms of acetylcholine and dopamine used to confirm the detection potentials in chronoamperometry experiments in Fig. 6B; control experiments for the simultaneous detection of dopamine and acetylcholine; simultaneous detection of acetylcholine (ACh) and dopamine (DA) using chronoamperometry on the dual-functional nano-carbon-ITIES electrode over a longer period of time; references. See DOI: **https://doi.org/10.1039/d4an01153h**

‡Current address: School of Chemistry and Chemical Engineering, Southeast University, Nanjing, 211189, China.

trode) has a nanoITIES electrode channel (for sensing non-redox-active analytes) and a carbon nanoelectrode channel (for detecting redox-active analytes), thus achieving multi-purpose analysis that is not possible with one type of electrode alone.

The introduced nano-carbon-ITIES electrodes expand on the current literature on multi-channel electrodes for multi-purpose analysis, which is an emerging area of research. Ewing *et al.* developed carbon microelectrode arrays as small as 10–50 μm to measure easily oxidizable substances.[48] Dick *et al.* incorporated a platinum disk working electrode (diameter = 25 μm), a platinum disk counter electrode (diameter = 25 μm), and a Ag/AgCl reference electrode into a triple-barrel probe.[49] Takami *et al.* developed sodium and potassium ion-selective electrodes in double-barrel glass pipettes at the size of 1 μm.[50] Shao *et al.* studied the heterogeneous electron-transfer reaction at the water/1,2-dichloroethane interface employing a double-barrel micropipette technique.[51]

In addition to the multi-purpose microprobes presented above, nanoscale theta pipettes have been developed into various platforms with powerful applications. Shao *et al.* developed both barrels as nanoITIES electrodes.[52] Unwin and Baker groups filled both barrels with aqueous electrolyte solutions for scanning electrochemical cell microscopy.[53–56] Baker *et al.* developed one barrel as a potential electrode and the second barrel as a scanning ion conductance microscopy probe.[57,58] Unwin, Wain, Matsue, Korchev and colleagues developed one barrel as carbon/platinum electrodes for scanning electrochemical microscopy (SECM) and the second barrel as the SICM probe.[59–62]

Adding to these pioneering studies, our study is the first to develop theta nanopipettes into nano-carbon-ITIES electrodes with one barrel functioning as an ITIES electrode and the second barrel functioning as a solid carbon nanoelectrode to detect non-redox-active and redox-active analytes, respectively.

After the development and characterization of the nano-carbon-ITIES electrode, in order to test its capability to measure both redox-active and non-redox-active analytes, we studied the detection of a non-redox-active analyte, acetylcholine (ACh), and a redox-active analyte, dopamine (DA), on the nano-carbon-ITIES electrode. ACh and DA are biologically and biomedically significant. ACh, the first neurotransmitter identified in 1914,[63,64] plays a key role in learning, memory and human health; defects in its release have been associated with aging and neurodegeneration.[28] DA is involved in memory, motor control, reward, and diseases such as Parkinson's disease and Schizophrenia.[13,65–70] Measuring ACh and DA at the same time is a cutting-edge area of research. Recent studies showed that both ACh and DA are involved in various diseases and disorders. For instance, besides ACh, dysfunction in DA has also been observed in Alzheimer's disease.[71–73] In addition, while DA has been extensively studied in drug addiction, the significant involvement of ACh was reported recently.[74] Thus, developing the analytical capability for the simultaneous detection of DA and ACh is important towards a better understanding of these diseases and disorders.

Here, we present the development and characterization of a dual-purpose nano-carbon-ITIES electrode for the first time. In addition, we demonstrated the simultaneous detection of both non-redox-active (acetylcholine) and redox-active (dopamine) analytes on the **nano-carbon-ITIES** electrode.

Results and discussion

Fabrication and characterization of the nano-carbon-ITIES platform

The nano-carbon-ITIES platform was developed based on dual-channel theta nanopipettes. We developed the theta nanopipette by laser pulling a theta capillary using a laser puller. Subsequently, we deposited carbon in one channel through pyrolysis and developed the second channel to be a nanoITIES electrode. We present below the fabrication and characterization of the dual-purpose nano-carbon-ITIES electrodes.

To develop the dual-channel theta nanopipette using a laser puller, we adjusted the pulling parameters and observed the pulled theta nanopipette using scanning electron microscopy (SEM) or transmission electron microscopy (TEM) until both channels of the theta nanopipette were open and of similar sizes. The optimized pulling parameters are Heat = 750, Fil = 4, Vel = 64, Del = 135, Pul = 79. SEM (Fig. 1A) and TEM (Fig. 1B) results showed we have successfully fabricated

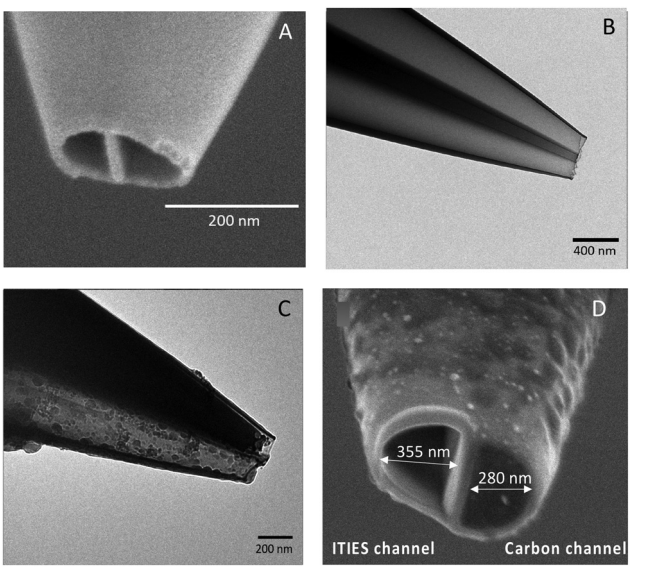

Fig. 1 (A) Scanning electron microscopic (SEM) and (B) transmission electron microscopic (TEM) images of the dual-channel theta nanopipettes, where smooth tip ends with nanometer-sized channels separated by a nanometer septum were observed. (C) TEM of the dual-channel nano-pipette after carbon deposition in one channel by pyrolysis where no significant changes in the geometry of the tip end was observed. (D) SEM image of the carbon-deposited dual-channel electrode after FIB milling of a second type of electrodes where changes in the geometry of the tip end were observed. The SEM image before FIB milling is shown in Fig. S1a.† SEM images were captured when the electrode was at a tilt angle of 52° from the horizontal plane.

theta nanopipettes with two nanometer-sized channels separated by nanometer-scale septa. Both nanochannels of the theta nanopipette were open and exhibited a relatively smooth surface.

To develop nano-carbon-ITIES electrode, we modified one channel of the theta nanopipette to be a carbon nanoelectrode by pyrolysis of acetylene, while the other channel was developed into a nanoITIES electrode (Fig. 2). The procedure of pyrolysis was modified based on the methods reported in the literature.[62,75–77] Detailed procedures were described under Experimental section.

After carbon deposition in one channel of the theta nanopipette *via* pyrolysis, we used TEM and SEM to observe the carbon-deposited dual-channel nanoprobe. Variations were observed depending on the deposition conditions. For instance, TEM results in Fig. 1C indicated that after carbon deposition, only one channel was filled with carbon while the second channel remained open. In addition, in the carbon-filled channel, the carbon was deposited close to the tip end, with no apparent deposition outside the probe. However, for another researcher, a change in the tip end of the dual-channel probe was observed after carbon deposition *via* pyrolysis (Fig. S1a†). In this case, we used focused ion beam (FIB) to mill the carbon-deposited dual-channel probe to generate a flat probe. The SEM result in Fig. 1D confirmed that after FIB milling, a smooth dual-channel nanoprobe has been successfully generated.

After carbon deposition and FIB milling, the carbon nanoelectrode channel of the nano-carbon-ITIES platform was characterized using cyclic voltammetry (CV) based on hexaammineruthenium (RuHex) reduction. The CV corresponding to RuHex reduction measured on the carbon nanoelectrode channel showed a sigmoidal shape (Fig. S2a†) as expected for nanoelectrodes.

Detection of dopamine (DA) on the carbon nanoelectrode of the dual-functional nano-carbon-ITIES platform

After the electrochemical characterization using the standard reduction mediator (RuHex) (ESI, section S2†), we performed DA detection studies on the carbon nanoelectrode channel of the nano-carbon-ITIES electrode. Electrochemical cell with cell diagram shown below was used for the DA detection, where ASW is the background solution.

$$\text{Cell 1}: \quad \text{Ag|AgCl|KCl (1 M)||ASW} + x \text{ mM DA|Carbon}$$

The cyclic voltammogram (CVs) of the background electrolyte, ASW, is shown in Fig. 3A (grey curve). After adding DA to the ASW, CVs with sigmoidal shapes corresponding to the DA detection were observed (additional CVs measured on different electrodes are provided in ESI, Fig. S3†). As more DA was added, current corresponding to DA detection increased. Diffusion-limited current at 0.40 V *vs.* Ag/AgCl/KCl (1 M) was used to construct the calibration curve (Fig. 3B). As shown in Fig. 3B, a linear relationship was observed between the diffusion-limited current and DA concentration, with the square of correlation coefficient (R^2) of 0.98. The linear range of detection appears to be from 0.1 mM to 0.5 mM. The size of the carbon nanoelectrode was calculated based on the cyclic voltammogram of RuHex to have a semicircular radius (a) of ~518 nm (ESI, section 2†). The semicircular radius was defined in Fig. 2B.

Looking closely at Fig. 3B, there appears to be a slight deviation from the linear line at a higher concentration (*e.g.*, 0.4 mM and 0.5 mM). To better visualize possible changes in the shape of the cyclic voltammograms at high DA concentrations, we normalized the current in the cyclic voltammograms by the diffusion-limiting current at 0.40 V *vs.* Ag/AgCl/KCl (1 M) with results shown in Fig. 4. Results in Fig. 4 revealed a slight change in the shape of the cyclic voltammograms at 0.3 mM (green dashed line) and 0.5 mM DA (black dotted line) with respect to 0.1 mM DA (red solid line).

Considering the very small current (pA) measured at the nanoelectrode, this shape change in cyclic voltammograms is less likely to be attributed to ohmic potential (current times solution resistance). Thus, these slight changes in the shape of cyclic voltammograms at 0.3 mM and 0.5 mM of dopamine may be attributed to carbon electrode fouling-related electrode surface modification.[78–81] Such modifications on the electrode

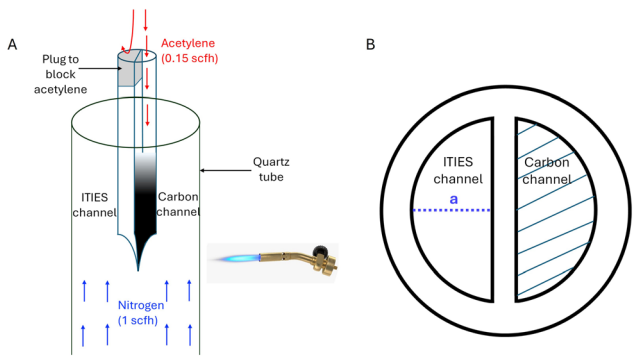

Fig. 2 (A) Schematic diagram of carbon deposition on one channel of the theta nanopipette to develop the carbon nanoelectrode while leaving the second channel open to be developed as a nanoITIES electrode. (B) Schematic diagram of the dual-functional nano-carbon-ITIES electrode with shape like that observed using SEM.

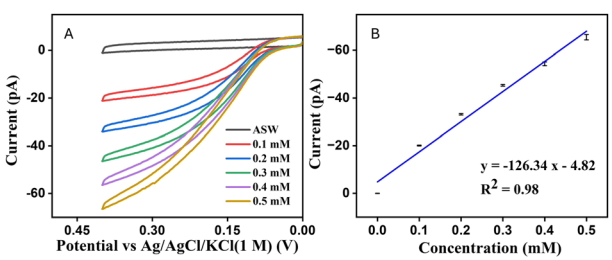

Fig. 3 (A) The cyclic voltammograms of dopamine (DA) detection on the carbon nanoelectrode channel of the nano-carbon-ITIES electrode. Different concentrations of DA were shown in the figure. (B) The calibration curve of DA detection. The average of the forward current measured at 0.4 V *vs.* Ag/AgCl/KCl (1 M) was used for the calibration curve. Artificial sea water (ASW) is the background electrolyte.

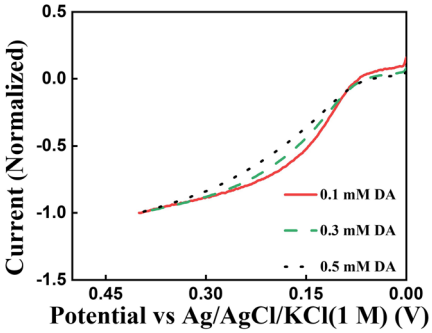

Fig. 4 Normalized forward scan of cyclic voltammograms in Fig. 3 of DA detection on the carbon nanoelectrode channel by its diffusion-limiting current at 0.4 V *vs.* Ag/AgCl/KCl (1 M).

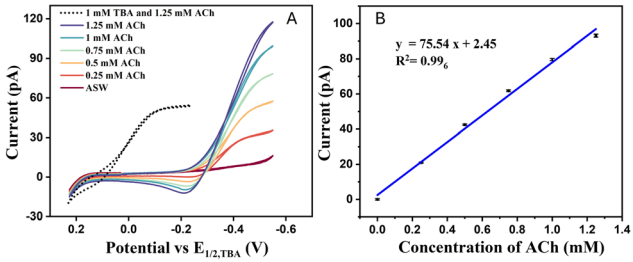

Fig. 5 (A) The cyclic voltammograms of acetylcholine (ACh) detection at the nanoITIES electrode of the dual-purpose nano-carbon-ITIES electrode. Different concentrations of ACh were shown in the figure. TBA (black dotted curve) was used as an internal standard and the cyclic voltammograms of ACh detection were plotted against the $E_{1/2,\ TBA}$. (B) The calibration curve of ACh detection. The average of the forward current measured at −0.5 V *vs.* $E_{1/2,\ TBA}$ was used for the calibration curve. Artificial sea water (ASW) is the background electrolyte.

surface may affect the kinetics of electrochemical reaction, which is shown as a change in the shape of steady-state cyclic voltammogram.[81,82]

The measured $E_{1/2}$ of DA detection was calculated to be 0.108 V ± 0.013 (n = 5) *vs.* Ag/AgCl/KCl (1 M) based on cyclic voltammograms of 0.1 or 0.2 mM DA detection (ESI, Table S2, Fig. S4 and section 5). We did not calculate the $E_{1/2}$ at higher concentrations of DA considering the possibility of electrode fouling. We further compared our $E_{1/2}$ of DA to that of the literature CV, which employed an Ag/AgCl wire in Tris buffer. Since the Ag/AgCl reference electrode depends on the concentration of Cl^- based on Nernst Equation, we calculated the chloride ion concentration in the Tris buffer to be 163.05 mM, and further calculated the potential of Ag/AgCl/Tris buffer to be 0.269 V. The $E_{1/2}$ of dopamine in this literature paper was 0.094 *vs.* Ag/AgCl/Tris buffer. The reference electrode we are using is Ag/AgCl/KCl (1 M), which has a potential of 0.222 V. Based on the above, the $E_{1/2}$ of DA in this literature paper is calculated to be 0.141 V *vs.* Ag/AgCl/KCl (1 M) from the cyclic voltammogram of 0.1 mM DA on a carbon fiber microelectrode.[83] This number is very close to what we observed, 0.108 V ± 0.013 *vs.* Ag/AgCl/KCl (1 M). The small difference might be related to the differences in carbon materials, since it was reported that the type of the carbon surface affects the dopamine oxidation reaction kinetics.[84]

Detection of acetylcholine (ACh) on the nanoITIES electrode channel of the dual-functional nano-carbon-ITIES platform

After FIB milling of the carbon-deposited dual-channel nanoprobe, we developed the non-carbon channel into a nanoITIES electrode using established procedures in PI's lab[12–14,25,28–31,35,85–89] with details described under Experimental section. In order to demonstrate the capability of the nanoITIES electrode channel for sensing non-redox-active analytes, we studied the detection of a non-redox-active neurotransmitter, ACh, on the nanoITIES electrode channel. We studied ACh detection quantitatively using cyclic voltammetry, with results shown in Fig. 5.

The cyclic voltammogram of the cellular background, ASW, is shown in Fig. 5A (brown curve). After we added ACh into the background solution, cyclic voltammograms with sigmoidal shapes were observed. As shown in Fig. 5A, the diffusion-limited current increased with increasing concentration of ACh. We added tetrabutylammonium (TBA) (as a standard) at the end of ACh detection experiment with the aim to report ACh detection potential with respect to half-wave detection potential of TBA, $E_{1/2}^{TBA}$. Cyclic voltammogram of TBA detection was shown as black dotted line in Fig. 5A.

We calculated the $E_{1/2,\ ACh}$ to be −0.34 V *vs.* $E_{1/2,\ TBA}$. We further compared this to the literature value. In the literature, $E_{1/2,\ ACh}$ was reported relative to $E_{1/2,\ TEA}$ (TEA, tetraethylammonium, another standard internal reference ion commonly used in ITIES studies).[87] In the current study, we used TBA as an internal standard. To enable direct comparison to the literature,[87] we conducted experiments to determine $E_{1/2,\ TBA}$ relative to $E_{1/2,\ TEA}$, with $E_{1/2,\ TBA} - E_{1/2,\ TEA}$ = 0.24 V. We further converted the literature value of $E_{1/2,\ ACh}$ *vs.* $E_{1/2,\ TEA}$ to $E_{1/2,\ ACh}$ *vs.* $E_{1/2,\ TBA}$. After conversion, the literature $E_{1/2}$ of ACh *vs.* $E_{1/2,\ TBA}$ is around −0.35 V. Our measured $E_{1/2,\ ACh}$ of −0.34 V *vs.* $E_{1/2,\ TBA}$ is in good agreement with the literature value of −0.35 V *vs.* $E_{1/2,\ TBA}$.[87]

We further constructed a calibration curve (Fig. 5B) by plotting the background-subtracted diffusion-limited current (at −0.5 V *vs.* $E_{1/2,\ TBA}$) as a function of the concentration of ACh. A linear correlation was observed between the diffusion-limited current and ACh concentration with an R^2 value of 0.99. This linear correlation between the diffusion-limited current and the concentration is expected based on the theory.[16,90] The electrode size was calculated from the steady state current of TBA transfer at the nanoITIES electrode with more details in section 4 of ESI.† The electrochemical semicircular radius (a) (defined in Fig. 2) was calculated to be ~419 nm.

Simultaneous detection of non-redox-active (acetylcholine) and redox-active (dopamine) analytes on the dual-functional nano-carbon-ITIES electrode

We hypothesize that the nano-carbon-ITIES electrode we have developed is capable of measuring both non-redox-active and

redox-active analytes at the same time. To test this hypothesis, we used acetylcholine (ACh) as one example of non-redox-active analyte and dopamine (DA) as one example of redox-active analyte. We exposed the nano-carbon-ITIES electrode to their solution mixture and recorded the current measured on the nanoITIES and carbon nanoelectrode channels, simultaneously.

To expose the nano-carbon-ITIES electrode to the mixture of ACh and DA, we injected a mixture of ACh and DA into the background electrolyte. The ACh and DA mixture was injected through an injection pipette towards the nano-carbon-ITIES electrode (Fig. 6A) with experimental details described under Experimental section. A Fast Green FCF dye was added to the solution mixture of ACh and DA to visualize the injected solution. The side-view optical microscopic images of the dual-functional nano-carbon-ITIES (DNCI) electrode, injection electrode and the injected mixture of ACh and DA were shown in Fig. 6B. In Fig. 6B, reflections of DNCI and injection pipette can be seen on the silicon wafer substrate. These reflections were used for the rough positioning of these probes.

As shown in Fig. 6A and B, we positioned the nano-carbon-ITIES electrode near the injection pipette, which was achieved using the positioner of a scanning electrochemical microscope (SECM) assisted by a lab-built side-view optical microscope. The position of the injection pipette was adjusted in such a way that the injected mixture of ACh and DA passed through the nano-carbon-ITIES electrode. This experimental setup needs to be further improved, *e.g.*, by improving the injection system, for the accurate determination of response time in the current-time response.

The simultaneous detection of ACh and DA on the nano-carbon-ITIES platform was studied by monitoring current on both nanocarbon and nanoITIES channels as a function of time, using chronoamperometry. To measure ACh and DA at the same time, we connected the two leads of the nanoITIES electrode and the carbon nanoelectrode to the green and yellow working electrode leads of a CHI SECM bipotentiostat, respectively. Two different potentials were applied on the nanoITIES and nano-carbon electrodes for the detection of ACh and DA, respectively. NanoITIES and carbon nanoelectrode channels were biased at −0.30 V and 0.30 V, respectively *vs.* Ag/AgCl/KCl (1 M). The applied potentials were where ACh and DA detection were observed in their corresponding cyclic voltammograms (ESI, Fig. S5 and section 6†).

The simultaneous detection of ACh and DA is shown in Fig. 6C. Dopamine detection is in blue (*y*-axis, left) and acetylcholine detection is in red (*y*-axis, right). The *x*-axis is the time and the arrows indicate the injection of dopamine and acetylcholine solution mixture. Current-time results over a longer period of time is shown in Fig. S8.†

As shown in Fig. 6C, the current responses for ACh and DA detection appears to be synchronized. For instance, following the injection of ACh and DA mixture at ~200 s, an increase in the current magnitude corresponding to ACh detection (red curve, *y*-axis on the right) was observed. Similarly, an increase in the current magnitude corresponding to DA detection (blue curve, *y*-axis on the left) was observed. After a brief plateau, ACh detection current decayed back to the baseline (red curve), so does the DA detection current (blue curve). This decrease in current was related to the dilution of the ACh and DA mixture solution. To confirm this is not coincidental, a longer injection of the ACh and DA mixture was applied, where we hypothesize to expect a longer plateau at the highest current magnitude. Results in Fig. 6C starting around 220 s showed that ACh detection current (red curve) and DA detection current (blue curve) followed a similar change, both exhibiting a longer plateau. Similar trends were observed with repeated injections. These observations that ACh detection and DA detection exhibited a similar current-time profile suggested their simultaneous detection.

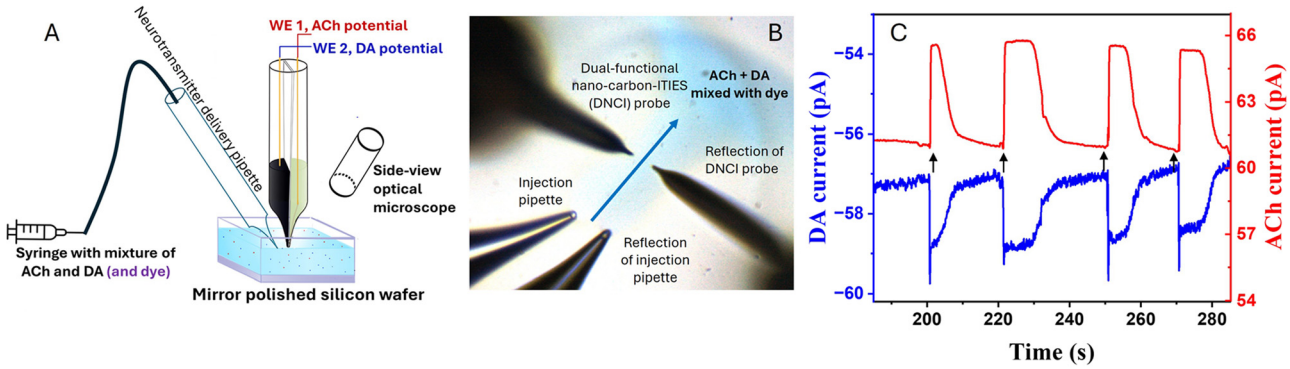

Fig. 6 Simultaneous detection of acetylcholine (ACh) and dopamine (DA) using chronoamperometry (current *vs.* time) on the nano-carbon-ITIES electrode. (A) The schematic diagram of the experimental setup, where a solution mixture of ACh and DA was injected from the injection pipette towards the nano-carbon-ITIES electrode. Fast green dye was added to aid in visualizing the injected solution and was imaged using lab-built side-view optical microscope. (B) The microscopic image of the experimental setup, where a solution mixture of ACh and DA was injected from the injection pipette towards the nano-carbon-ITIES electrode. Fast green dye was added to aid in visualizing the injected solution. The reflections were used to guide the rough positioning of both injection pipette and nano-carbon-ITIES electrode. (C) Current-time traces measured on the nanoITIES and nano-carbon electrode channels following the injection of a mixture of DA and ACh. Black arrows indicate the injection of dopamine and acetylcholine mixture.

In addition, we conducted control experiments by biasing the carbon nanoelectrode and nanoITIES electrode of the dual-purpose nano-carbon-ITIES platform at potentials where neither DA nor ACh were measurable (ESI, Fig. S7 and section 7†), and we did not observe any current peaks. These results confirm the simultaneous detection of ACh and DA on the nano-carbon-ITIES electrode.

Experimental

Materials and supplies

Sodium chloride (NaCl) was from EMD Chemicals (Gibbstown, NJ). Potassium chloride (KCl) was from VWR International (Radnor, PA). Magnesium chloride hexahydrate ($MgCl_2 \cdot 6H_2O$) was from Amresco (Solon, OH). Magnesium sulfate ($MgSO_4$) and HEPES were from Fischer Scientific (Pittsburgh, PA). Calcium chloride dihydrate ($CaCl_2 \cdot 2H_2O$), tetradodecylammonium (TDDA) chloride, tetrabutylammonium chloride (TBACl), cupric acetate ($Cu(OAc)_2$), 1,2-dichloroethane (DCE), *N*,*N*-dimethyltrimethylsilylamine, dopamine hydrochloride and acetylcholine chloride were purchased from Sigma-Aldrich (St Louis, MO). The TFAB salt of TDDA (TDDATFAB) was prepared by metathesis, as described elsewhere.[13,14,25,28,30,35,85,86,91] Ethanol (190 Proof) used for catalysis solution was purchased from Decon Laboratories (King of Prussia, PA). Hexaammineruthenium chloride (RuHex) used for the characterization of carbon nanoelectrode was purchased from Strem Chemicals (Newburyport, MA). All the aqueous solutions were made with 18.3 MΩ cm deionized water. Artificial seawater (ASW) which contains the following: 460 mM NaCl, 10 mM KCl, 10 mM $CaCl_2$, 22 mM $MgCl_2$, 26 mM $MgSO_4$ and 10 mM HEPES (pH 7.8) in 18.3 MΩ cm deionized water was used as the aqueous background electrolyte solution. Dental wax and the wall mounting putty was purchased from HRASY and Scotch (St Paul, MN), respectively. Conductive silver epoxy was from Ted Pella (Redding, CA). We used ASW as the background electrolyte for the *in vitro* detection considering that ASW is the cellular medium of a commonly-studied neuronal model, *Aplysia californica*.[28–30,89]

A transmission electron microscope (TEM) (Philips CM200, FEI Co., Hillsboro, OR) and a scanning electron microscope (SEM) (FEI Helios 600i Dual-Beam SEM/FIB, FEI Co., Hills-boro, OR) were used to characterize the nanopipette after pulling and after carbon deposition by pyrolysis. Pipettes were coated with gold and palladium mixture of 3 : 2 composition using a sputter coater (Emitech K575, Emitech Ltd, Ashford, Kent) under 20 mA current for 45 s before SEM. Sputter coating increases the resolution of the images obtained using SEM by mitigating charging on the glass pipette surface, thereby reducing blurring.[31] SEM images were captured under a 2 kV electron beam with a beam current of 43 pA. FEI Helios 600i Dual-Beam SEM/FIB was also used to mill the pyrolyzed dual-channel pipettes to make the surface smooth as needed. All electrochemical measurements were performed using a CHI920D or CHI760e potentiostat (CHI Instruments, Austin, TX).

Dual-functional nano-carbon-ITIES electrode fabrication and characterization

The dual-functional nanoelectrode, developed from dual-channel nanopipettes, is composed of a nanoITIES channel and a second channel filled with carbon through pyrolysis. The dual-channel nanopipettes were fabricated by laser pulling quartz capillaries (outer diameter = 1.2 mm, inner diameter = 0.9 mm, length = 7.5 cm, Sutter Instrument Co., Novato, CA) with a P-2000 capillary puller (Sutter Instrument Co., Novato, CA).

After pulling, one channel of the nanopipette was modified to be a carbon nanoelectrode by pyrolysis, while the other channel was developed into a nanoITIES electrode. The procedure of pyrolysis was modified based on the methods reported in the literature.[62,75–77] Briefly, one channel of the nanopipette was backfilled with a cupric acetate solution, *i.e.*, 5 mg cupric acetate in 7.5 ml of 1 : 1 mixture of ethanol and water. Solvent of catalysis solution was dried off from the nanopipettes by heating at 70 °C under vacuum. $Cu(OAc)_2$ was reported to serve as a precursor of catalyst to grow carbon nanomaterials.[92–94]

Following the drying of the catalyst solution, the ITIES channel was blocked with a plug made of 1 : 1 mixture of wall mounting putty and dental wax as illustrated in Fig. 2. Subsequently, the nanopipettes were connected to an acetylene source at the top of the pipette. These nanopipettes were positioned inside a quartz tubing through which nitrogen gas was flowed upward, as indicated by the blue arrows in Fig. 2. Inert nitrogen gas was employed to prevent the oxidation of the carbon layer, bending of the capillary at high temperatures, and the closing of the pipette aperture due to the softening of the quartz walls.[62,77] During pyrolysis, acetylene was passed through the unblocked channel, and a propane flame torch was used to heat the outside of the sheathing quartz tube for carbon deposition. Piloting studies were carried out to find the best condition for carbon deposition in one channel of the dual-channel nanopipette. The method of pyrolysis was modified from the earlier reported methods by adding flow meters to the pyrolysis station to allow accurate control of gas flow of both acetylene and nitrogen.

The following protocol has been developed for depositing carbon in the dual-functional nanoelectrodes of sizes reported in this work. Procedure modification would be needed for nanoelectrodes of different sizes. The acetylene flow rate was maintained at 0.15 standard cubic feet per hour (scfh) while the nitrogen flow rate was kept at 1 scfh. The heating consisted of four heating steps of 60 s (in total 240 s), with a 30 s cooling period between each step. After pyrolysis, a copper wire was inserted and fixed into the carbon-filled channel using conductive silver epoxy for electrical connection. The dual-channel nanopipette was later subjected to focused ion beam milling to obtain a flat carbon electrode as needed. During fabrication process, the carbon channel was handled with care to prevent electrostatic discharge damage to the carbon nanoelectrode using methods reported.[95,96]

To develop the non-carbon filled channel to be an ITIES electrode, the plug was removed from the blocked channel, and nanoITIES electrode was developed using our previously established procedures as detailed below.[13,25,28,30,35,86,87] The surface of the quartz pipette was rendered hydrophobic through chemical vapor silanization using *N*,*N*-dimethyltrimethylsilylamine.[16,30,85,87,89,97] This surface modification is crucial for establishing a stable aqueous/organic interface at the electrode orifice. The nanoITIES channel was backfilled with an organic solution of 5 mM TDDATFAB dissolved in DCE with a 10 μL Hamilton syringe. The filling solution was forced to the nanotip using gentle vibrations created by tapping with a serrated tweezer. An etched Pt wire was inserted into the DCE solution and was positioned close from the tip end. The platinum wire's position was secured using the dental wax.

Electrochemical measurements

The detection of DA and ACh were studied on the carbon nanoelectrode and nanoITIES channel, respectively, with cyclic voltammetry (CV) and chronoamperometry. A three-electrode configuration was employed, with the commercial Ag/AgCl/KCl (1 M) electrode serving as the outer reference electrode. A salt bridge was used to connect the outer reference electrode to artificial seawater (ASW) background electrolyte solution. A tungsten wire was used as the outer counter electrode. NanoITIES electrode serves as the working electrode for ACh detection. The scan rate for the CVs of both background and ACh is 0.025 V s^{-1}. Upon applying a negative potential to the nanoITIES channel with respect to the reference electrode, the positively charged ions in the aqueous phase transfer to the organic phase, generating a positive current. The sign convention for the current and potential follows previous studies.[85,87,98] For the electrochemical reaction on the carbon nanoelectrode channel, we followed the convention in the "Electrochemical Methods, Fundamentals and Applications" by A. J. Bard, L. R. Faulkner and H. S. White,[99] where oxidation is measured as a positive current. Carbon nanoelectrode channel served as the working electrode for DA detection. The scan rate for the background CV was 0.02 V s^{-1}, and for DA CVs was 0.0175 V s^{-1}. The double layer charging background current is proportional to the scan rate, and ideally the same scan rate should be used in the background and dopamine CVs. However, after a close look at the data, the capacitive current from 0–0.05 V between the background (scan rate: 0.02 V s^{-1}) and dopamine (scan rate: 0.0175 V s^{-1}, 0.1 and 0.2 mM) are pretty similar. Considering this, we used the background current measured at 0.02 V s^{-1} as an estimation for background subtraction in calibration curve of DA detection.

Simultaneous detection of DA and ACh was conducted using chronoamperometry. During simultaneous detection, the carbon nanoelectrode channel was connected to the green lead (working electrode 1), and the nanoITIES channel was connected to the yellow lead (working electrode 2) of a CHI920D bi-potentiostat. Tetrabutylammonium (TBA) was added at the end of nanoITIES experiments, so ACh transfer potential with respect to the half wave transfer potential of TBA, $E_{TBA,\ 1/2}$, was reported. During electrochemical measurements, the carbon channel was handled with care to prevent electrostatic discharge damage, following procedures reported.[95,96]

In vitro simultaneous detection of redox-active (dopamine) and non-redox-active (acetylcholine) analytes

We dosed out a mixture of dopamine and acetylcholine near the nano-carbon-ITIES electrode to test its capability to measure both analytes at the same time. We used injection micropipettes connected to a 5 mL syringe containing dopamine and acetylcholine *via* teflon tubing to inject out the analyte mixture. The analyte mixture was dosed out manually using finger pressure to push the syringe loaded with dopamine and acetylcholine. The analyte mixture was composed of 0.4 mM DA, 0.4 mM ACh and Fast Green FCF Dye (Sigma Aldrich, St Louis, MO) in ASW. Prior to usage, we filtered the analyte mixture using a 0.2 μm filter (Thermo Scientific, Waltham, MA). Fast Green FCF Dye was added to the mixture solution to visualize it using a lab-built side-view optical microscope and verify the accurate application of the injected solution.

Micropipettes used above had outer radii of ~20–21 μm and were fabricated *via* laser pulling of borosilicate capillaries (Sutter Instrument Co., Novato, CA; outer diameter = 1.0 mm, inner diameter = 0.50 mm, length = 10 cm), with a P-2000 capillary puller (Sutter Instrument Co., Novato, CA), with the following pulling parameters:

$$\text{Heat} = 260, \text{Fil} = 4, \text{Vel} = 18, \text{Del} = 220, \text{Pul} = 0.$$

Conclusion

We have developed and characterized a nanometer scale dual-purpose platform, *i.e.*, nano-carbon-ITIES electrodes, to measure both redox-active and non-redox-active analytes. The nano-carbon-ITIES electrode was developed based on a dual-channel theta nanopipette. We laser pulled theta capillaries to generate dual-channel theta nanopipettes with both sides open and of similar sizes. We developed one channel as a carbon nanoelectrode by carbon deposition *via* pyrolysis and the second channel as a nanoITIES electrode. We demonstrated the quantitative detection of acetylcholine (a non-redox-active neurotransmitter) on the nanoITIES electrode and dopamine (a redox-active neurotransmitter) on the carbon nanoelectrode of the nano-carbon-ITIES electrode using cyclic voltammetry. On both electrode channels, diffusion-limited current increased linearly with increasing concentrations of acetylcholine and dopamine. We measured dopamine and acetylcholine simultaneously on the nano-carbon-ITIES electrode by measuring current as a function of time *in vitro*. It is worth to note that there is still room for improvement. While we have shown in Table S1 (C, D and E)† that geometric area determined using SEM and electrochemical area of fresh FIB-

milled carbon nanoelectrode were rather close, there were some other electrodes where a smaller electrochemical current was generated with respect to the size measured using SEM (Fig. S3, A1 and A2†). Regardless, the presented first-ever nano-carbon-ITIES platform expands current analytical capability in multi-modal analysis by integrating the functionality a solid carbon nanoelectrode (for sensing redox-active analytes), and a nano liquid/liquid junction ITIES electrode (for detecting non-redox-active analytes), thus achieving multi-purpose analysis that is not possible with one type of electrode alone.

Author Contributions

E. S. Anupriya: conceptualization, methodology, validation, data collection, formal data analysis, data curation, writing-original draft preparation, writing-review & editing, visualization. R. Chen: writing-part of original draft, methodology, transmission electron microscopy data collection. D. Kalski: methodology, table of content graphics. J. Palmer: methodology. M. Shen: conceived the idea, supervision of the project, conceptualization, methodology, writing-original draft preparation, writing-review & editing, data analysis, visualization, project administration and funding acquisition. All authors except D.K. (a former undergraduate student and cannot be reached) reviewed the manuscript.

Data availability

The data presented in this study are available on request from the corresponding author. The data supporting this article have been included as part of the ESI.†

Conflicts of interest

There are no conflicts to declare.

Acknowledgements

We are grateful for the support of this research by a USA National Science Foundation CAREER Award (CHE 19-45274) and Alfred P. Sloan Fellowship (FG-2023-20536) to M. Shen. We thank Dr Honghui Zhou for the helpful discussions for the SEM studies. We thank Dr Joaquín Rodríguez-López and Dr Zachary T. Gossage for their help in building the pyrolysis station. The SEM and FIB experiments were carried out in the Materials Research Laboratory Central Research Facilities, University of Illinois Urbana-Champaign. TEM experiments were carried out in the Beckman Institute for Advanced Science and Technology at University of Illinois Urbana-Champaign.

References

1 G. D. Sisk, G. Herzog, J. D. Glennon and D. W. Arrigan, Assessment of ion transfer amperometry at liquid–liquid interfaces for detection in CE, *Electrophoresis*, 2009, **30**(19), 3366–3371.
2 Z. Samec, Dynamic electrochemistry at the interface between two immiscible electrolytes, *Electrochim. Acta*, 2012, **84**, 21–28.
3 H. H. Girault, Electrochemistry at liquid–liquid interfaces, *Electroanal. Chem.*, 2010, **23**, 1–104.
4 P. Vanýsek and L. Basáez Ramírez, Interface between two immiscible liquid electrolytes: a review, *J. Chil. Chem. Soc.*, 2008, **53**(2), 1455–1463.
5 Y. Shao and M. V. Mirkin, Voltammetry at Micropipet Electrodes, *Anal. Chem.*, 1998, **70**(15), 3155–3161.
6 F. Reymond, D. Fermın, H. J. Lee and H. H. Girault, Electrochemistry at liquid/liquid interfaces: methodology and potential applications, *Electrochim. Acta*, 2000, **45**(15–16), 2647–2662.
7 T. Solomon and A. J. Bard, Scanning electrochemical microscopy. 30. Application of glass micropipet tips and electron transfer at the interface between two immiscible electrolyte solutions for SECM imaging, *Anal. Chem.*, 1995, **67**(17), 2787–2790.
8 J. Koryta, Electrochemical polarization phenomena at the interface of two immiscible electrolyte solutions, *Electrochim. Acta*, 1979, **24**(3), 293–300.
9 D. Homolka, L. Q. Hung, A. Hofmanova, M. Khalil, J. Koryta, V. Marecek, Z. Samec, S. Sen and P. Vanysek, Faradaic ion transfer across the interface of two immiscible electrolyte solutions: chronopotentiometry and cyclic voltammetry, *Anal. Chem.*, 1980, **52**(11), 1606–1610.
10 Z. Samec, V. Mareček, J. Koryta and M. Khalil, Investigation of ion transfer across the interface between two immiscible electrolyte solutions by cyclic voltammetry, *J. Electroanal. Chem. Interfacial Electrochem.*, 1977, **83**(2), 393–397.
11 V. Mareček and Z. Samec, Ion transfer kinetics at the interface between two immiscible electrolyte solutions supported on a thick-wall micro-capillary. A mini review, *Curr. Opin. Electrochem.*, 2017, **1**(1), 133–139.
12 C. B. Milton, K. Xu and M. Shen, Recent advances in nanoelectrochemistry at the interface between two immiscible electrolyte solutions, *Curr. Opin. Electrochem.*, 2022, **34**, 101005.
13 M. L. Colombo, S. McNeil, N. Iwai, A. Chang and M. Shen, Electrochemical detection of dopamine via assisted ion transfer at nanopipet electrode using cyclic voltammetry, *J. Electrochem. Soc.*, 2015, **163**(4), H3072–H3076.
14 M. L. Colombo, J. V. Sweedler and M. Shen, Nanopipet-Based Liquid–Liquid Interface Probes for the Electrochemical Detection of Acetylcholine, Tryptamine, and Serotonin via Ionic Transfer, *Anal. Chem.*, 2015, **87**(10), 5095–5100.
15 E. Bakker, Electroanalysis with membrane electrodes and liquid–liquid interfaces, *Anal. Chem.*, 2016, **88**(1), 395–413.

16 K. Alanis, S. E. Alden, L. A. Baker, E. S. Anupriya, H. D. Jetmore and M. Shen, Micro and nanopipettes for electrochemical imaging and measurement, in *Scanning Electrochemical Microscopy*, ed. A. J. Bard and M. V. Mirkin, CRC Press, 2022, pp. 419–480.
17 Y. Shao, Electrochemistry at liquid/liquid interfaces, in *Handbook of electrochemistry*, ed. C. G. Zoski, Elsevier, 2007, pp. 785–809.
18 Z. Samec, Electrochemistry at the interface between two immiscible electrolyte solutions (IUPAC Technical Report), *Pure Appl. Chem.*, 2004, **76**(12), 2147–2180.
19 S. Amemiya, Y. Wang and M. V. Mirkin, Nanoelectrochemistry at the liquid/liquid interfaces, in *Electrochemistry*, Vol. 12: Nanoelectrochemistry, P. De Richemont, ed. R. G. Compton and J. D. Wadhawan, The Royal Society of Chemistry, 2013, pp. 1–43.
20 S. Amemiya, J. Kim, A. Izadyar, B. Kabagambe, M. Shen and R. Ishimatsu, Electrochemical sensing and imaging based on ion transfer at liquid/liquid interfaces, *Electrochim. Acta*, 2013, **110**, 836–845.
21 Y. Liu, R. Moshrefi, W. D. Rickard, M. D. Scanlon, T. J. Stockmann and D. W. Arrigan, Ion-transfer electrochemistry at arrays of nanoscale interfaces between two immiscible electrolyte solutions arranged in hexagonal format, *J. Electroanal. Chem.*, 2022, **909**, 116113.
22 M. D. Scanlon, E. Smirnov, T. J. Stockmann and P. Peljo, Gold nanofilms at liquid–liquid interfaces: an emerging platform for redox electrocatalysis, nanoplasmonic sensors, and electrovariable optics, *Chem. Rev.*, 2018, **118**(7), 3722–3751.
23 T. J. Stockmann, R. Guterman, P. J. Ragogna and Z. Ding, Trends in hydrophilicity/lipophilicity of phosphonium ionic liquids as determined by ion-transfer electrochemistry, *Langmuir*, 2016, **32**(49), 12966–12974.
24 T. J. Stockmann, A.-M. Montgomery and Z. Ding, Determination of alkali metal ion transfers at liquid| liquid interfaces stabilized by a micropipette, *J. Electroanal. Chem.*, 2012, **684**, 6–12.
25 N. T. Iwai, M. Kramaric, D. Crabbe, Y. Wei, R. Chen and M. Shen, GABA Detection with Nano-ITIES Pipet Electrode: A New Mechanism, Water/DCE-Octanoic Acid Interface, *Anal. Chem.*, 2018, **90**(5), 3067–3072.
26 B. Liu and M. V. Mirkin, Voltammetry at Micro-ITIES, in *Liquid Interfaces In Chemical, Biological And Pharmaceutical Applications*, ed. A. G. Volkov, CRC Press, 2001, pp. 455–486.
27 Z. Samec, E. Samcová and H. H. Girault, Ion amperometry at the interface between two immiscible electrolyte solutions in view of realizing the amperometric ion-selective electrode, *Talanta*, 2004, **63**(1), 21–32.
28 M. Shen, Z. Qu, J. Deslaurier, T. M. Welle, J. V. Sweedler and R. Chen, Single Synaptic Observation of Cholinergic Neurotransmission on Living Neurons: Concentration and Dynamics, *J. Am. Chem. Soc.*, 2018, **140**(25), 7764–7768.
29 R. Chen, K. Alanis, T. M. Welle and M. Shen, Nanoelectrochemistry in the study of single-cell signaling, *Anal. Bioanal. Chem.*, 2020, **412**, 6121–6132.
30 T. M. Welle, K. Alanis, M. L. Colombo, J. V. Sweedler and M. Shen, A high spatiotemporal study of somatic exocytosis with scanning electrochemical microscopy and nanoITIES electrodes, *Chem. Sci.*, 2018, **9**(22), 4937–4941.
31 M. Shen and M. L. Colombo, Electrochemical nanoprobes for the chemical detection of neurotransmitters, *Anal. Methods*, 2015, **7**(17), 7095–7105.
32 A. Berduque, R. Zazpe and D. W. Arrigan, Electrochemical detection of dopamine using arrays of liquid–liquid micro-interfaces created within micromachined silicon membranes, *Anal. Chim. Acta*, 2008, **611**(2), 156–162.
33 V. Beni, M. Ghita and D. W. M. Arrigan, Cyclic and pulse voltammetric study of dopamine at the interface between two immiscible electrolyte solutions, *Biosens. Bioelectron.*, 2005, **20**(10), 2097–2103.
34 D. W. Arrigan, M. Ghita and V. Beni, Selective voltammetric detection of dopamine in the presence of ascorbate, *Chem. Commun.*, 2004, (6), 732–733.
35 H. D. Jetmore, C. B. Milton, E. S. Anupriya, R. Chen, K. Xu and M. Shen, Detection of Acetylcholine at Nanoscale NPOE/Water Liquid/Liquid Interface Electrodes, *Anal. Chem.*, 2021, **93**(49), 16535–16542.
36 M. M. Ahmed, F. S. Bodowara, W. Zhou, J. F. Penteado, J. L. Smeltz and P. Pathirathna, Electrochemical detection of Cd (ii) ions in complex matrices with nanopipets, *RSC Adv.*, 2022, **12**(2), 1077–1083.
37 Y. Yuan and Y. Shao, Systematic investigation of alkali metal ion transfer across the micro-and nano-water/1, 2-dichloroethane interfaces facilitated by dibenzo-18-crown-6, *J. Phys. Chem. B*, 2002, **106**(32), 7809–7814.
38 Y. Kitatsuji, Z. Yoshida, H. Kudo and S. Kihara, Transfer of actinide ion at the interface between aqueous and nitrobenzene solutions studied by controlled-potential electrolysis at the interface, *J. Electroanal. Chem.*, 2002, **520**(1–2), 133–144.
39 A. Benvidi, S. N. Lanjwani and Z. Ding, Facilitated proton transfer by 2-acetylpyridine-4-phenyl-3-thiosemicarbazone across water/1, 2-dichloroethane interface, *J. Electroanal. Chem.*, 2010, **641**(1–2), 99–103.
40 S. Chesniuk, S. Dassie, L. Yudi and A. Baruzzi, Electrochemical study of the interaction of alkali and alkaline-earth cations with a dibehenoyl phosphatidylcholine monolayer at the water/1, 2-dichloroethane interface, *Electrochim. Acta*, 1998, **43**(14–15), 2175–2181.
41 H. R. Kim, C. M. Pereira, H. Y. Han and H. J. Lee, Voltammetric studies of topotecan transfer across liquid/liquid interfaces and sensing applications, *Anal. Chem.*, 2015, **87**(10), 5356–5362.
42 S. R. Puri and J. Kim, Kinetics of antimicrobial drug ion transfer at a water/oil interface studied by nanopipet voltammetry, *Anal. Chem.*, 2019, **91**(3), 1873–1879.
43 J. A. Ribeiro and C. M. Pereira, Applications of Electrochemistry at the ITIES in Drug Discovery and Development–A Review, *ChemElectroChem*, 2024, **11**(13), e202400134.

44 S. O'Sullivan and D. W. Arrigan, Electrochemical behaviour of myoglobin at an array of microscopic liquid–liquid interfaces, *Electrochim. Acta*, 2012, **77**, 71–76.
45 D. W. Arrigan, M. J. Hackett and R. L. Mancera, Electrochemistry of proteins at the interface between two immiscible electrolyte solutions, *Curr. Opin. Electrochem.*, 2018, **12**, 27–32.
46 G. Herzog and D. W. Arrigan, Electrochemical strategies for the label-free detection of amino acids, peptides and proteins, *Analyst*, 2007, **132**(7), 615–632.
47 G. Herzog, A. Roger, D. Sheehan and D. W. Arrigan, Ion-transfer voltammetric behavior of protein digests at liquid|liquid interfaces, *Anal. Chem.*, 2010, **82**(1), 258–264.
48 Y. Lin, R. Trouillon, M. I. Svensson, J. D. Keighron, A.-S. Cans and A. G. Ewing, Carbon-ring microelectrode arrays for electrochemical imaging of single cell exocytosis: fabrication and characterization, *Anal. Chem.*, 2012, **84**(6), 2949–2954.
49 P. J. Kauffmann, N. L. Walker, V. Gupta and J. E. Dick, Triple-Barrel Ultramicroelectrodes for Multipurpose, Submilliliter Electroanalysis, *Anal. Chem.*, 2023, **95**(22), 8411–8416.
50 T. Takami, Y. Akutsu, N. Kaneko, R. Yoneda, H. Magara, S. Ogawa and T. Abukawa, Development of Dual Ion-selective Electrodes in Double-Barrel Glass Pipette at One Micrometer for Simultaneous Measurement of Sodium and Potassium Ions, *e-J. Surf. Sci. Nanotechnol.*, 2022, **21**(1), 17–23.
51 Y. Chen, Z. Gao, F. Li, L. Ge, M. Zhang, D. Zhan and Y. Shao, Studies of electron-transfer and charge-transfer coupling processes at a liquid/liquid interface by double-barrel micropipet technique, *Anal. Chem.*, 2003, **75**(23), 6593–6601.
52 H. Hu, S. Xie, X. Meng, P. Jing, M. Zhang, L. Shen, Z. Zhu, M. Li, Q. Zhuang and Y. Shao, Fabrication and characterization of submicrometer-and nanometer-sized double-barrel pipets, *Anal. Chem.*, 2006, **78**(19), 7034–7039.
53 N. Ebejer, M. Schnippering, A. W. Colburn, M. A. Edwards and P. R. Unwin, Localized high resolution electrochemistry and multifunctional imaging: Scanning electrochemical cell microscopy, *Anal. Chem.*, 2010, **82**(22), 9141–9145.
54 A. G. Güell, A. S. Cuharuc, Y.-R. Kim, G. Zhang, S.-y. Tan, N. Ebejer and P. R. Unwin, Redox-dependent spatially resolved electrochemistry at graphene and graphite step edges, *ACS Nano*, 2015, **9**(4), 3558–3571.
55 M. Choi, N. P. Siepser, S. Jeong, Y. Wang, G. Jagdale, X. Ye and L. A. Baker, Probing single-particle electrocatalytic activity at facet-controlled gold nanocrystals, *Nano Lett.*, 2020, **20**(2), 1233–1239.
56 S. Jeong, M.-H. Choi, G. S. Jagdale, Y. Zhong, N. P. Siepser, Y. Wang, X. Zhan, L. A. Baker and X. Ye, Unraveling the structural sensitivity of CO2 electroreduction at facet-defined nanocrystals via correlative single-entity and macroelectrode measurements, *J. Am. Chem. Soc.*, 2022, **144**(28), 12673–12680.
57 C.-C. Chen, Y. Zhou, C. A. Morris, J. Hou and L. A. Baker, Scanning ion conductance microscopy measurement of paracellular channel conductance in tight junctions, *Anal. Chem.*, 2013, **85**(7), 3621–3628.
58 Y. Zhou, C.-C. Chen, A. E. Weber, L. Zhou and L. A. Baker, Potentiometric-scanning ion conductance microscopy, *Langmuir*, 2014, **30**(19), 5669–5675.
59 M. A. O'Connell and A. J. Wain, Mapping electroactivity at individual catalytic nanostructures using high-resolution scanning electrochemical–scanning ion conductance microcopy, *Anal. Chem.*, 2014, **86**(24), 12100–12107.
60 M. Şen, Y. Takahashi, Y. Matsumae, Y. Horiguchi, A. Kumatani, K. Ino, H. Shiku and T. Matsue, Improving the electrochemical imaging sensitivity of scanning electrochemical microscopy-scanning ion conductance microscopy by using electrochemical Pt deposition, *Anal. Chem.*, 2015, **87**(6), 3484–3489.
61 A. Page, M. Kang, A. Armitstead, D. Perry and P. R. Unwin, Quantitative visualization of molecular delivery and uptake at living cells with self-referencing scanning ion conductance microscopy-scanning electrochemical microscopy, *Anal. Chem.*, 2017, **89**(5), 3021–3028.
62 Y. Takahashi, A. I. Shevchuk, P. Novak, Y. Zhang, N. Ebejer, J. V. Macpherson, P. R. Unwin, A. J. Pollard, D. Roy and C. A. Clifford, Multifunctional nanoprobes for nanoscale chemical imaging and localized chemical delivery at surfaces and interfaces, *Angew. Chem., Int. Ed.*, 2011, **50**(41), 9638–9642.
63 H. H. Dale, The action of certain esters and ethers of choline, and their relation to muscarine, *J. Pharmacol. Exp. Ther.*, 1914, **6**(2), 147–190.
64 O. Loewi, Über humorale übertragbarkeit der Herznervenwirkung, *Pflügers Arch*, 1921, **189**(1), 239–242.
65 A. De Iuliis, E. Montinaro, G. Fatati, M. Plebani and C. Colosimo, Diabetes mellitus and Parkinson's disease: dangerous liaisons between insulin and dopamine, *Neural Regener. Res.*, 2022, **17**(3), 523.
66 A. Björklund and S. B. Dunnett, Fifty years of dopamine research, *Trends Neurosci.*, 2007, **30**(5), 185–187.
67 S. D. Iversen and L. L. Iversen, Dopamine: 50 years in perspective, *Trends Neurosci.*, 2007, **30**(5), 188–193.
68 B. Boilly, S. Faulkner, P. Jobling and H. Hondermarck, Nerve dependence: from regeneration to cancer, *Cancer Cell*, 2017, **31**(3), 342–354.
69 A. C. Michael and L. Borland, *Electrochemical methods for neuroscience*, CRC press, 2006.
70 A. C. Michael and G. S. Wilson, *Compendium of in Vivo Monitoring in Real-time Molecular Neuroscience: Probing brain function, disease and injury with enhanced optical and electrochemical sensors*, World Scientific, 2019.
71 E. Spoleti, L. La Barbera, E. Cauzzi, M. L. De Paolis, L. Saba, R. Marino, G. Sciamanna, V. Di Lazzaro, F. Keller and A. Nobili, Dopamine neuron degeneration in the Ventral Tegmental Area causes hippocampal hyperexcitability in experimental Alzheimer's Disease, *Mol. Psychiatry*, 2024, **29**(5), 1265–1280.
72 A. Nobili, E. C. Latagliata, M. T. Viscomi, V. Cavallucci, D. Cutuli, G. Giacovazzo, P. Krashia, F. R. Rizzo, R. Marino

and M. Federici, Dopamine neuronal loss contributes to memory and reward dysfunction in a model of Alzheimer's disease, *Nat. Commun.*, 2017, **8**(1), 14727.

73 Y. Gloria, K. Ceyzériat, S. Tsartsalis, P. Millet and B. B. Tournier, Dopaminergic dysfunction in the 3xTg-AD mice model of Alzheimer's disease, *Sci. Rep.*, 2021, **11**(1), 19412.

74 M. J. Williams and B. Adinoff, The role of acetylcholine in cocaine addiction, *Neuropsychopharmacology*, 2008, **33**(8), 1779–1797.

75 Z. T. Gossage, B. H. Simpson, N. B. Schorr and J. Rodríguez-López, Soft surfaces for fast characterization and positioning of scanning electrochemical microscopy nanoelectrode tips, *Anal. Chem.*, 2016, **88**(20), 9897–9901.

76 Z. J. Barton and J. Rodríguez-López, Lithium ion quantification using mercury amalgams as in situ electrochemical probes in nonaqueous media, *Anal. Chem.*, 2014, **86**(21), 10660–10667.

77 P. Actis, S. Tokar, J. Clausmeyer, B. Babakinejad, S. Mikhaleva, R. Cornut, Y. Takahashi, A. López Córdoba, P. Novak and A. I. Shevchuck, Electrochemical nanoprobes for single-cell analysis, *ACS Nano*, 2014, **8**(1), 875–884.

78 A. Kousar, E. Peltola and T. Laurila, Nanostructured geometries strongly affect fouling of carbon electrodes, *ACS Omega*, 2021, **6**(40), 26391–26403.

79 Y. Y. Lau, J. B. Chien, D. K. Wong and A. G. Ewing, Characterization of the voltammetric response at intracellular carbon ring electrodes, *Electroanalysis*, 1991, **3**(2), 87–95.

80 S. Chandra, A. D. Miller and D. K. Wong, Evaluation of physically small p-phenylacetate-modified carbon electrodes against fouling during dopamine detection in vivo, *Electrochim. Acta*, 2013, **101**, 225–231.

81 N. Nioradze, R. Chen, N. Kurapati, A. Khvataeva-Domanov, S. Mabic and S. Amemiya, Organic contamination of highly oriented pyrolytic graphite as studied by scanning electrochemical microscopy, *Anal. Chem.*, 2015, **87**(9), 4836–4843.

82 E. Peltola, S. Sainio, K. B. Holt, T. Palomäki, J. Koskinen and T. Laurila, Electrochemical fouling of dopamine and recovery of carbon electrodes, *Anal. Chem.*, 2018, **90**(2), 1408–1416.

83 P. Pathirathna, R. J. Balla and S. Amemiya, Nanogap-based electrochemical measurements at double-carbon-fiber ultramicroelectrodes, *Anal. Chem.*, 2018, **90**(20), 11746–11750.

84 A. N. Patel, S.-y. Tan, T. S. Miller, J. V. Macpherson and P. R. Unwin, Comparison and reappraisal of carbon electrodes for the voltammetric detection of dopamine, *Anal. Chem.*, 2013, **85**(24), 11755–11764.

85 R. Chen, K. Xu and M. Shen, Avocado oil, coconut oil, walnut oil as true oil phase for ion transfer at nanoscale liquid/liquid interfaces, *Electrochim. Acta*, 2020, **357**, 136788.

86 R. Chen, A. Yang, A. Chang, P. F. Oweimrin, J. Romero, P. Vichitcharoenpaisarn, S. Tapia, K. Ha, C. Villaflor and M. Shen, A Newly Synthesized Tris(crown ether) Ionophore for Assisted Ion Transfer at NanoITIES Electrodes, *ChemElectroChem*, 2020, **7**(4), 967–974.

87 M. L. Colombo, J. V. Sweedler and M. Shen, Nanopipet-based liquid-liquid interface probes for the electrochemical detection of acetylcholine, tryptamine, and serotonin via ionic transfer, *Anal. Chem.*, 2015, **87**(10), 5095–5100.

88 H. D. Jetmore, E. S. Anupriya, T. J. Cress and M. Shen, Interface between two immiscible electrolyte solutions electrodes for chemical analysis, *Anal. Chem.*, 2022, **94**(48), 16519–16527.

89 M. Shen and R. Chen, *Real time studies of acetylcholine release from single synapses and single cells with nanometer spatial resolution, Compendium of in vivo monitoring in real-time molecular neuroscience*, ed. G. S. Wilson and A. C. Michael, World Scientific, Singapore, 2019, pp. 161–178.

90 C. Lefrou, A unified new analytical approximation for positive feedback currents with a microdisk SECM tip, *J. Electroanal. Chem.*, 2006, **592**(1), 103–112.

91 J. Guo and S. Amemiya, Voltammetric heparin-selective electrode based on thin liquid membrane with conducting polymer-modified solid support, *Anal. Chem.*, 2006, **78**(19), 6893–6902.

92 J. N. Wang, L. F. Su and Z. P. Wu, Growth of highly compressed and regular coiled carbon nanotubes by a spray-pyrolysis method, *Cryst. Growth Des.*, 2008, **8**(5), 1741–1747.

93 R. L. Vander Wal, T. M. Ticich and V. E. Curtis, Substrate–support interactions in metal-catalyzed carbon nanofiber growth, *Carbon*, 2001, **39**(15), 2277–2289.

94 W. Zhou, Z. Han, J. Wang, Y. Zhang, Z. Jin, X. Sun, Y. Zhang, C. Yan and Y. Li, Copper catalyzing growth of single-walled carbon nanotubes on substrates, *Nano Lett.*, 2006, **6**(12), 2987–2990.

95 R. Chen, K. Hu, Y. Yu, M. V. Mirkin and S. Amemiya, Focused-ion-beam-milled carbon nanoelectrodes for scanning electrochemical microscopy, *J. Electrochem. Soc.*, 2015, **163**(4), H3032–H3037.

96 N. Nioradze, R. Chen, J. Kim, M. Shen, P. Santhosh and S. Amemiya, Origins of nanoscale damage to glass-sealed platinum electrodes with submicrometer and nanometer size, *Anal. Chem.*, 2013, **85**(13), 6198–6202.

97 M. Shen, R. Ishimatsu, J. Kim and S. Amemiya, Quantitative imaging of ion transport through single nanopores by high-resolution scanning electrochemical microscopy, *J. Am. Chem. Soc.*, 2012, **134**(24), 9856–9859.

98 E. S. Anupriya and M. Shen, New Method in Surface Treatment of Nanopipette for Interface between Two Immiscible Electrolyte Solutions (ITIES) Experiment, *J. Electrochem. Soc.*, 2022, **169**(4), 046501.

99 A. J. Bard, L. R. Faulkner and H. S. White, *Electrochemical methods: fundamentals and applications*, John Wiley & Sons, 2022.

